Chirp Spread Spectrum as a Modulation Technique for Long Range Communication

Brecht Reynders, Sofie Pollin
Department of Electrical Engineering
KU Leuven
Heverlee, B-3001 Belgium
Email: brecht.reynders@esat.kuleuven.be, sofie.pollin@esat.kuleuven.be

***Abstract*—Long range low power is a family of technologies promising to connect thousands of sensors to the future internet of things. Within this family of possible technology choices, two different branches have emerged: the standards based on spreaded wideband communication and the standards based on narrowband communication, both promising to reach long range connectivity at very low power. More specifically, this paper focuses on chirp spread spectrum (CSS). This paper presents a detailed model of CSS, showing that the symbols are not perfectly orthogonal. The results show the potential communication ranges are close to narrowband networks and the robustness against interfering signals is 22 dB better for spreading factor 10 than BPSK. Although wideband communication is robust to interference, in long range communication, this robustness is insufficient due to the long range and the larger footprint. The large propagation losses due to the long range and the larger footprint make CSS prone to collisions with other noise sources, possibly larger than the coding gain.**

I. Introduction

Long range communication or low power wide area networks (LPWANs) are networks where high data rate requirements are traded for range and energy improvements. In these networks, data rates are very low, leaving hardly a few bytes per seconds, but enabling ranges of a few kilometers.

In our previous paper [1], we have compared two such LPWANs: an ultra narrowband, Sigfox-like standard with a wideband, LoRa-like technology. This paper elaborates more on our detailed model of the physical layer of CSS and prove that the spreading factors are not perfectly orthogonal.

This paper is definitely not the first paper to evaluate the LoRa standard. Many papers have been published. However, most of them rely on measurements in the field to derive physical layer properties [2], [3]. The authors of these papers measured the reliability of the link at different distances form the base station for different spreading factors. In [4], the authors combine the information from the datasheet of a LoRa transceiver to identify the capacity and range constraints in these networks. An analysis of orthogonal chirp spread spectrum is given in [5], however, where orthogonal symbols are achieved by relying on both up and down-chirps. A detailed analysis of the CSS-symbols used LoRa with different sources of noise and interference is missing.

This paper gives an extended insight in the performance of chirp spread spectrum. Whenever possible, CSS will be compared to narrowband communications like the BPSK used in SigFox [6]. More specifically, the coverage and the coexistence with other competing signals in the same band will be taken in consideration. Coexistence is an important parameter because of the unlicensed bands these networks typically use. The remainder of this paper is structured as follows. The first section summarizes the real world model we used in our simulations. The next section gives a detailed overview of the technology and the model we implemented in Matlab. Section IV shows the results of our simulations and model. And finally, this paper ends with a small discussion about higher layers and the conclusion.

II. Model

For our range simulations, some assumption have been made. First, the noise is assumed to be just thermal noise. The equation for the noise power P_n is shown in Eq. 1 with T the temperature in Kelvin (25^{o}C), k the constant of Boltzmann and B the bandwidth. This noise power is the lower bound, as there will be other ambient noise sources in the ISM-band.

$$P_n = kTB \tag{1}$$

Second, the signal power decays with distance following the Hata model [7]. In this comparison, the model for urban areas is used as the highest number of devices will occur in these areas. The formula for losses in urban environment L is shown in Eq. 2. In this formula, d is the distance between base station and device in meter, f the frequency (868MHz), h_B the height of the base station in meter (30m), h_M the height of the mobile device (1m):

$$\begin{aligned} L = 69.55 + 26.16log_{10}(f) - 13.82log_{10}(h_B) \\ -3.2(log_{10}(11.54h_M))^2 \\ -4.97 + [44.9 - 6.55log_{10}(h_B)]log_{10}(d). \end{aligned} \tag{2}$$

Third, only the uplink is considered, as the majority of the data flows in this direction. The uplink data is modeled as packets with length l and l equals 160 bits or 20 bytes. Finally, the transmitter of the mobile device sends with a power of 25mW, which is the maximal allowed power in most of the ISM-band.

978-1-5090-4361-3/16/$31.00 2016 European Union

To investigate the coexistence, three different noise sources were used: additive white Gaussian noise (AWGN), a continuous wave and a CSS symbol with different spreading factor. The continuous wave interferer has, for each simulated symbol, a constant random frequency uniformly distributed between f_{min} and f_{max} (the minimal and maximal frequency of CSS) with a random phase offset, also uniformly distributed between 0 and 2π. Eq. 3 shows the equation for generating a CW $C(t)$. In this equation, a is the amplitude of the signal, t is the time, f is the constant frequency and ϕ is the constant phase offset.

$$C(t) = ae^{i(2\pi ft+\phi)} \tag{3}$$

Further, the transmitter and the receiver are assumed to be perfectly synchronized to enable coherent detection.

III. Chirp Spread Spectrum

Chirp spread spectrum is a technique known from the physical layer of LoRaWAN [8]. The standard uses chirp spread spectrum (CSS) as modulation to transmit over large distances in the 868MHz band. LoRaWAN includes a scalable bandwidth (125kHz, 250kHz or 500kHz). Based on the bandwidth and the SNR, a variable spreading factor is chosen to spread the signal to make it more robust to noise. The resulting bit rate will vary between 300bps and 37.5kbps. The used parameters will be mentioned in the evaluation section. The rest of this section introduces the CSS symbols in detail, proves that they are not perfectly orthogonal and finally, describes the decoder functionality assumed for the performance evaluation.

1) CSS symbols: A CSS symbol has four important parameters: the spreading factor S, the minimal frequency f_{min}, the maximal frequency f_{max} and the input bits. To generate a CSS symbol, a starting frequency f_0 is needed. The starting frequency, lying between f_{min} and f_{max}, represents the input information of $log_2(S)$ bits. For a spreading factor S[1], $log_2(S)$ bits define f_0. Then, the length of the symbol can be calculated. The length of one symbol t_s is shown in Eq. 4:

$$t_s = \frac{S}{B} = \frac{S}{f_{max} - f_{min}}, \tag{4}$$

where B is the bandwidth or the difference between f_{min} and f_{max}. From this formula, the bit rate $R_B(S)$ can be calculated:

$$R_b(S) = \frac{log_2(S)}{t_s} \tag{5}$$

When the symbol length is defined, the signal constantly chirps over all frequencies starting at f_0 to f_{max} and continuing from f_{min} to f_0. The mathematical representation is given in Eq. 6. The frequency in function of time $f(t)$ is also shown in Fig. 1.

$$s(t) = e^{i2\pi f(t)t}. \tag{6}$$

[1]It should be noted that the spreading factor is defined here as the amount of chips per symbol. This is different from the spreading factor used in the LoRaWAN specification or used in other papers. The value there equals the *SpreadingFactor* register value. For more information, [9] Sec. 4.1.1.2

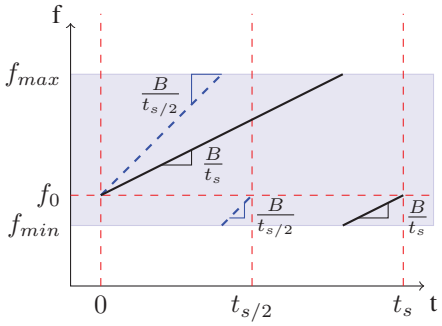

Fig. 1: Graphical representation of the frequency in time for two CSS symbols with spreading factor s and $s/2$.

Proposition 1. *Two CSS symbols are not guaranteed to be orthogonal.*

Proof. Assume two different CSS symbols $s_1(t)$ and $s_2(t)$ are orthogonal to each other, then Eq. 7 should hold:

$$\begin{aligned} 0 &= \int_0^{t_s} s_1^*(t)s_2(t)dt \\ &= \int_0^{t_s} e^{-i2\pi f_1(t)t}e^{i2\pi f_2(t)t}dt, \end{aligned} \tag{7}$$

where

$$f_i(t) = \begin{cases} \frac{B}{t_s}t + \frac{k_i}{S}B & x < t_i \\ \frac{B}{t_s}t + \frac{k_i}{S}B - B & x \geq t_i \end{cases} \tag{8}$$

with $i = 1, 2$, and k_1 and k_2 the different integer input symbols from 0 to $S-1$.

$$t_s\frac{S-k_i}{S} = t_i, i = 1, 2, \tag{9}$$

with t_1 and t_2 the times where respectively $s_1(t)$ and $s_2(t)$ switch from f_{max} to f_{min} shown in Fig. 1. Assume that $k_1 > k_2$ such that $0 \leq t_1 < t_2 \leq t_s$, then Eq. 7 becomes:

$$\begin{aligned} 0 = \int_0^{t_1} e^{-i2\pi\frac{k_1-k_2}{S}Bt}dt + \int_{t_1}^{t_2} e^{-i2\pi(\frac{k_1-k_2}{S}B-B)t}dt \\ + \int_{t_2}^{t_s} e^{-i2\pi\frac{k_1-k_2}{S}Bt}dt. \end{aligned} \tag{10}$$

Solving the integrals in Eq. 10 results in Eq. 11:

$$\begin{aligned} 0 =& \frac{i[e^{-i2\pi\frac{k_1-k_2}{S}B0} - e^{-i2\pi\frac{k_1-k_2}{S}Bt_1}]}{\frac{k_1-k_2}{S}B} \\ &+ \frac{i[e^{-i2\pi(\frac{k_1-k_2}{S}B-B)t_1} - e^{-i2\pi(\frac{k_1-k_2}{S}B-B)t_2}]}{\frac{k_1-k_2}{S}B - B} \\ &+ \frac{i[e^{-i2\pi\frac{k_1-k_2}{S}Bt_2} - e^{-i2\pi\frac{k_1-k_2}{S}Bt_s}]}{\frac{k_1-k_2}{S}B} \end{aligned} \tag{11}$$

Because k_1 and k_2 are not equal to each other and the difference can never be equal to S, we can rewrite the denominator. Including Eq. 9 in Eq. 11, gives:

$$\begin{aligned} 0 = (\frac{k_1-k_2}{S}B - B)[1 - e^{-i2\pi\frac{k_1-k_2}{S}Bt_s\frac{S-k_1}{S}} \\ + e^{-i2\pi\frac{k_1-k_2}{S}Bt_s\frac{S-k_2}{S}} - e^{-i2\pi\frac{k_1-k_2}{S}Bt_s}] \\ + (\frac{k_1-k_2}{S}B)[e^{-i2\pi(\frac{k_1-k_2}{S}B-B)t_s\frac{S-k_1}{S}} \\ - e^{-i2\pi(\frac{k_1-k_2}{S}B-B)t_s\frac{S-k_2}{S}}]. \end{aligned} \tag{12}$$

Combining Eq. 12 and Eq. 4, we show that

$$\begin{aligned} 0 = (\frac{k_1-k_2}{S}B - B)[1 - e^{-i2\pi\frac{k_1-k_2}{S}(S-k_1)} \\ + e^{-i2\pi\frac{k_1-k_2}{S}(S-k_2)} - e^{-i2\pi(k_1-k_2)}] \\ + (\frac{k_1-k_2}{S}B)[e^{-i2\pi(\frac{k_1-k_2}{S}-1)(S-k_1)} \\ - e^{-i2\pi(\frac{k_1-k_2}{S}-1)(S-k_2)}]. \end{aligned} \tag{13}$$

Because $e^{i2\pi k}$ with k integer is always 1, Eq. 13 yields:

$$\begin{aligned} 0 = (\frac{k_1-k_2}{S}B - B)[-e^{i2\pi\frac{k_1-k_2}{S}k_1} + e^{i2\pi\frac{k_1-k_2}{S}k_2}] \\ +(\frac{k_1-k_2}{S}B)[e^{i2\pi\frac{k_1-k_2}{S}k_1} - e^{i2\pi\frac{k_1-k_2}{S}k_2}] \end{aligned} \tag{14}$$

$$0 = e^{i2\pi\frac{k_1-k_2}{S}k_1} - e^{i2\pi\frac{k_1-k_2}{S}k_2} \tag{15}$$

$$= e^{i2\pi\frac{k_1-k_2}{S}k_2}(e^{i2\pi\frac{(k_1-k_2)^2}{S}} - 1) \tag{16}$$

Eq. 16 is only true if and only if the difference between k_1 and k_2 equals a multiple of the square root of the spreading factor. □

2) Decoding CSS symbols: Because the symbols are close to orthogonal, a decoder was designed that uses correlation to decode the signal. Every received symbol in the decoder is correlated with the base CSS symbols. The decoder makes a decision based on the maximum correlation.

Another possible decoder is presented in [10]. The authors in [10] propose to mix and resample the incoming symbol to create a clear shifted narrow peak in the frequency domain. Both decoder implementations however give the same performance with AWG noise.

IV. Simulation Results

This section shows the results of the implementation of our model to show the potential range and coexistence capabilities.

A. Bit error rate

Before estimating the potential range for a CSS based network, a closed-form equation for the bit error rate (BER) of CSS symbols with varying spreading factors is needed. For this, 10 000 symbols were generated for each SNR and decoded with the decoder proposed in III-2. The resulting points of this simulation were put in the curve fitting toolbox of MATLAB to estimate the BER curve for CSS. The results of this fit is shown for a CSS symbol with 10 bits in Fig. 3. Also the BER curve for a BPSK symbol with 1 bit per symbol (Eq. 17) [11] and an FSK symbol with k equal to 10 bits per symbol (Eq. 18) [12] are shown. To convert SNR to energy per bit to noise density (E_b/N_0), Eq. 20 was used, where P_s/P_n is the signal-to-noise ratio, B is the bandwidth and $R_b(S)$ is the bit rate.

$$P_{e,BPSK} = Q(\sqrt{2\frac{E_b}{N_0}}) \tag{17}$$

$$P_{e,FSK} = \frac{1}{\sqrt{8\pi}}\int_{-\infty}^{\infty}[1 - (\frac{1}{\sqrt{2\pi}}\int_{-\infty}^{y}\exp^{-x^2/2}\,dx)^{2^k-1}] \exp^{-\frac{1}{2}(y-\sqrt{\frac{2kE_b}{N_0}})^2}\,dy \tag{18}$$

This can be simplified as Eq. 19, proposed in [13].

$$P_{e,FSK} = \frac{2^k}{4}Q(\sqrt{k\frac{E_b}{N_0}}) \tag{19}$$

$$\frac{E_b}{N_0} = \frac{P_s B}{P_n R_b(S)} \tag{20}$$

$$P_{e,CSS} = \frac{1}{2}Q(1.28\sqrt{k\frac{E_b}{N_0}} - \sqrt{k}1.28 + 0.4) \tag{21}$$

It can be seen that both 10-bit FSK and 10-bit CSS have a BER that decreases faster with increasing SNR compared to BPSK. In FSK or any orthogonal constellation, it is possible to project each received symbol with noise to the signal space spanned by the 2^k orthogonal symbols. As it turns out, the received symbol will align perfectly in one direction (the direction of the corresponding symbol), while the noise will align with all the vectors in all directions. To decode, the maximal direction is selected. After mapping any 2 different orthogonal symbols in that 2^k dimensional space, we can observe that their distance only depends on their energy E_s. A higher E_s means they are further away and hence a lower probability of symbol and hence bit errors. In the case of antipodal symbols, it should be noticed that their signal space has only 2^{k-1} spanning symbols. So, some of the symbols lie on the same vector but with opposite sign. The distance between 2 symbols on the same vector is however larger. This is visualized for the case of 1 bit or 2 symbols in Fig. 2. From this figure, it should be clear that BFSK performs worse than BPSK as the distance between symbols is smaller. When orthogonal symbols are considered with more bits per symbol, the distance between the symbols determines the symbol error rate (SER). The energy per symbol E_s depends linearly on the energy per bit E_b and the amount of bits per symbol k, shown in Eq. 22. So, with a constant energy per bit, the symbol energy will scale linearly with k, resulting in a larger E_s and lower SER when k increases. As a result, the BER is lower too, as the average BER is 50% of the SER. This reasoning is only valid if the SNR is high enough and the symbol error rate is small. When the SNR is small, an increase in symbol energy will not lead to a lower SER. For low SNR, more bits just means more symbols and hence, more different values to pick from and to fail.

$$E_s = kE_b \tag{22}$$

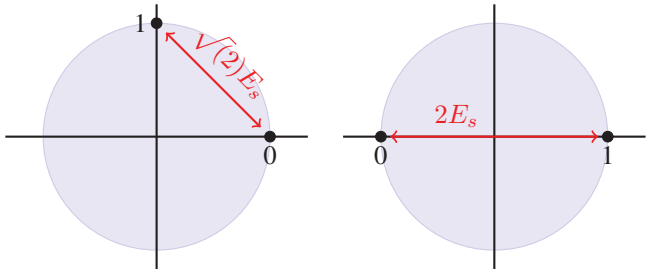

(a) BFSK or 2 orthogonal symbol

(b) BPSK or 2 antipodal symbol

Fig. 2: Difference in distance between 2 different symbols (0 and 1), when mapped to the signal space. It is clear that orthogonal symbols are closer together than antipodal symbols. If more bits are added, the distance between the orthogonal symbols stays the same. In PSK however, the symbols will be closer together.

We can observe this behavior also in the equation for FSK (Eq. 18). The latter part in the equation is the correlation of the correct wanted signal with noise, and this correlation needs to be compared to the correlations with the other $2^k - 1$ symbols shown in the first part of the equation. The equation shows that when E_b/N_0 is high, the first part goes to 0 in the significant region where y is around $\sqrt{2kE_b/N_0}$ and the SER for FSK is almost equal for all k, resulting in an advantage for symbols with more bits. When the SNR is low, more errors are observed because the probability is small that all the $2^k - 1$ different correlators give a lower value than the one of the wanted symbol. In the case of BPSK, the distance between the 2 symbols is larger, and hence, BPSK performs better for small SNR. So, the bit error curve of BPSK and the bit error curve of FSK for $k > 2$ cross.

For CSS, a similar reasoning could be followed. But here, the non-orthogonal symbols need to be taken into account. A constant offset should be introduced in each of the correlators depending on the symbol that was sent. To simplify the equation, Eq. 21 was estimated in Matlab with the simulated data. The simulated bit curves show a square root over energy per bit and contain a constant part that is only function of the number of bits inside each symbol. The latter term is the result of the non-orthogonality proven in Sec. 1.

B. Range

When taken into account the wider bandwidth and the higher bit rate, CSS results in a smaller coverage area. This can be seen in figure 4. The figure shows the throughput of both physical layers based on the packet error. The equation of the throughput is given in Eq. 23. In this formula, P_p is the probability of a packet error and can be calculated with Eq. 24 with P_e the probability of a bit error described in previous section. In this simulation, we did not take into account the scalable data rate provided in LoraWAN, but only used the most reliable spreading factor. It should be noticed here, that for the sensor side, a CSS network is preferred, as the range is almost the same, but close to the base station, a higher throughput can be achieved. The latter results in shorter messages and less power consumption.

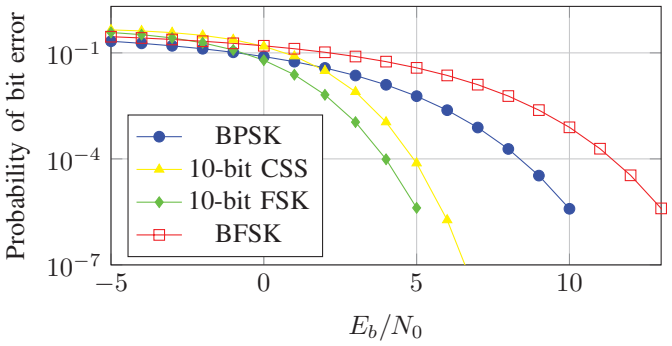

Fig. 3: Bit error rate of a BPSK, CSS symbol with bandwidth 125kHz with 10 bits and FSK symbol with 10 bits. For lower values of E_b/N_0, BPSK gives better results, but for higher values, CSS is better.

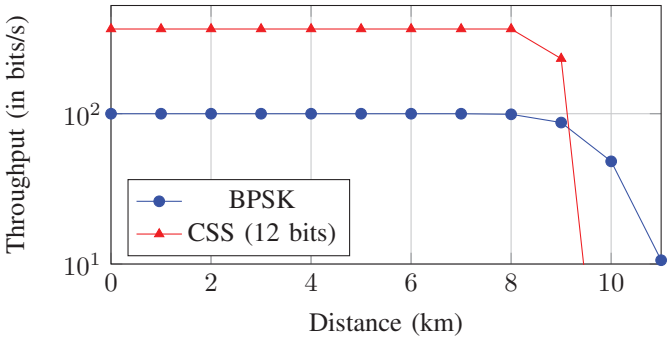

Fig. 4: Throughput of BPSK (sigfox-like) and CSS network based on the range. The range of an UNB network is larger than the CSS network.

$$T = (1 - P_P)R_B \tag{23}$$

$$P_p = 1 - (1 - P_e)^l \tag{24}$$

C. Coexistence

Figure 5 shows the robustness of CSS (Eq. 6) against a continuous wave (Eq. 3) with a given SIR (defined as Eq. 25). A wideband symbol as CSS needs a certain SIR to be able to spread the interferer over it's bandwidth. For spreading factor 10, that SINR equals $-16dB$. Higher spreading factors require less and lower more SINR.

In a second simulation, also shown in figure 5, a CSS-symbol is demodulated while another CSS-symbol with different spreading factor is present. For spread spectrum systems, the demodulator should be able to ignore symbols with different spreading factors. This can be verified by the figure

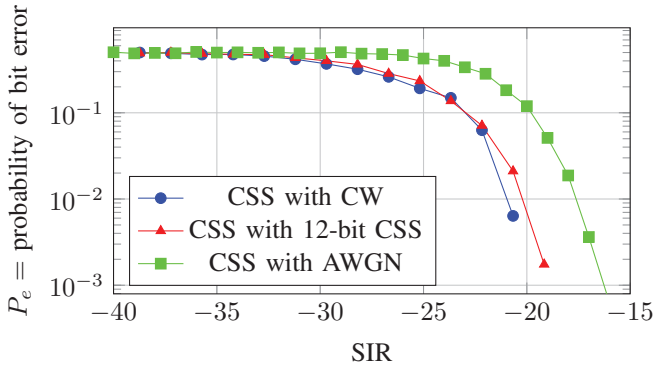

Fig. 5: BER for CSS symbol and LoRa symbol with 10 bits per symbol and bandwidth $B = 500kHz$.

because both the curve of a continuous wave as the one from another spreading factor are close. the CSS-demodulator sees the other CSS symbol with a different spreading as modulated noise, like the continuous wave. This feature allows to send simultaneously to the same base station with good power control and different spreading factors.

$$SIR = 10log_{10}(\frac{P_{signal}}{P_{interferer}}) = -20log(a_i) \qquad (25)$$

It should be obvious that coexistence in CSS is more powerful than coexistence in BPSK-based networks as described in [14]. For maximal BER of 10^{-3}, 22 dB less power is required for CSS based networks.

V. Discussion

There are three important insights that need to be emphasized. First, CSS is indeed robust against interference due to the spreading, but the time-bandwidth footprint is significantly bigger than BPSK. This makes it more prone to multiple interfering sources and get the SINR below the threshold.
Secondly, it should be noted that 16 dB is small if you take into account the possible link budget of 150 dB. If a competing device is significantly closer to the base station, the packet from the far away node will not arrive at all even when colliding with a packet with a different spreading factor.
The final remark related to the overall network throughput. From [15] and [16], we can estimate the overall throughput in the network. As LoRaWAN uses unslotted aloha, the equations of [15] apply. The maximal network throughput occurs when on average $1/2$ packet with spreading factor S is sent during the transmission of one packet ($l/R_b(S)$ with both parameters defined above) with the same spreading factor with a packet delivery ratio (PDR) of $1/e$. This can be summed over different spreading factor assuming they do not interfere each other. The BPSK network is narrowband and can hence use B/b channels to have the same bandwidth, where b is the BPSK bandwidth (100 Hz). The authors in [16] show that the maximal network throughput occurs when on average $1/4$ packet is sent per channel during the transmission of one packet (l/R_S with $R_S = 100$ bps) with a PDR of $1/e$. This is summarized in Eq. 26 and Eq. 27. These equations show that overall a BPSK network can send four times as many messages then a CSS network. Adding more spreading factors to increase the throughput is possible, but these small spreading factors are very sensitive to noise and require a higher SINR.

$$T_{CSS} = \frac{1}{2e}\sum_{i=7}^{12}[\frac{R_b(S)}{l}] \Rightarrow T_{CSS} = 18packets/s \qquad (26)$$

$$T_{UNB} = \frac{1}{4e}\frac{R_S}{l}\frac{B}{b} \qquad \Rightarrow T_{UNB} = 72packets/s \qquad (27)$$

VI. Conclusion

This paper showed a detailed analysis of chirp spread spectrum. The symbols in CSS are not perfectly orthogonal. The simulation results show that it is suited for LPWAN, and the communication range is close to the ranges narrowband solutions can reach. But, there is an advantage of 22dB in coexistence and robustness against interference compared to BPSK for spreading factor 10. Although CSS is robust against interference and has a scalable data rate, the time-bandwidth footprint is significantly higher than the footprint of the narrowband solution. This results that for the entire network, it is preferred to have a narrowband solution.

References

[1] B. Reynders *et al.*, "Range and coexistence analysis of long range unlicensed communication," in *Telecommunications (ICT), 2016 23rd International Conference on*. IEEE, 2016, pp. 1–6.

[2] S. Kartakis *et al.*, "Demystifying low-power wide-area communications for city iot applications," in *Proceedings of the Tenth ACM International Workshop on Wireless Network Testbeds, Experimental Evaluation, and Characterization*, ser. WiNTECH '16. New York, NY, USA: ACM, 2016, pp. 2–8. [Online]. Available: http://doi.acm.org/10.1145/2980159.2980162

[3] M. Centenaro *et al.*, "Long-Range Communications in Unlicensed Bands: the Rising Stars in the IoT and Smart City Scenarios," *IEEE Wireless Communications*, vol. 23, October 2016.

[4] K. Mikhaylov *et al.*, "Analysis of capacity and scalability of the lora low power wide area network technology," in *European Wireless 2016; 22th European Wireless Conference; Proceedings of*. VDE VERLAG GmbH, 2016, pp. 1–6.

[5] A. Springer *et al.*, "Spread spectrum communications using chirp signals," in *EUROCOMM 2000. Information Systems for Enhanced Public Safety and Security. IEEE/AFCEA*. IEEE, 2000, pp. 166–170.

[6] "Sigfox," http://www.sigfox.com/en, 2014, accessed: 2015-02-01.

[7] M. Hata, "Empirical formula for propagation loss in land mobile radio services," *Vehicular Technology, IEEE Transactions on*, vol. 29, no. 3, pp. 317–325, 1980.

[8] *LoRaWAN Specification*, LoRa Alliance, Inc, Jan. 2015, rev. 1.

[9] *860 MHz to 1020 MHz Low Power Long Range Transceiver*, Semtech Corporation, 2014, rev. 2.

[10] C. Goursaud and J. M. Gorce, "Dedicated networks for iot: Phy / mac state of the art and challenges," *EAI Endorsed Transactions on Internet of Things*, vol. 15, no. 1, 10 2015.

[11] L. W. Couch, II, *Digital and Analog Communication Systems*, 6th ed. Upper Saddle River, NJ, USA: Prentice Hall PTR, 2000.

[12] J. G. Proakis, "Digital communications fourth edition, 2001," 1998.

[13] A. RF, "Link budget analysis: Digital modulation, part," http://www.atlantarf.com/FSK_Modulation.php, 2013, accessed: 2015-08-23.

[14] R. Axford, "Effects of cw-and bpsk-signal interference on a standard bpsk digital communications system," DTIC Document, Tech. Rep., 1992.

[15] A. S. Tanenbaum, "Computer networks. 5th," 2011.

[16] C. Goursaud and Y. Mo, "Random unslotted time-frequency aloha: Theory and application to iot unb networks," in *Telecommunications (ICT), 2016 23rd International Conference on*. IEEE, 2016, pp. 1–5.